Grain Refinement of Freeform Fabricated Ti-6Al-4V Alloy Using Beam/Arc Modulation

Scott Mitzner[a], Stephen Liu[a], Marcia Domack[b], Robert Hafley[b]

Abstract

Grain refinement can significantly improve the mechanical properties of freeform-fabricated Ti-6Al-4V alloy, promoting increased strength and enhanced isotropy compared with coarser grained material. Large β-grains can lead to a segregated microstructure, in regard to both α-phase morphology and α-lath orientation. Beam modulation, which has been used in conventional fusion welding to promote grain refinement, is explored in this study for use in additive manufacturing processes including electron beam freeform fabrication (EBF^3) and gas-tungsten arc (GTA) deposition to alter solidification behavior and produce a refined microstructure. The dynamic molten pool size induced by beam modulation causes rapid heat flow variance and results in a more competitive grain growth environment, reducing grain size. Consequently, improved isotropy and strength can be achieved with relatively small adjustments to deposition parameters.

[a] Colorado School of Mines, Golden, CO
[b] NASA Langley Research Center, Hampton, VA

Key words: Ti-6Al-4V alloy, grain refinement, electron beam, gas-tungsten arc, freeform fabrication

Introduction

Solid freeform fabrication (SFF) is an additive manufacturing process in which material is added to a substrate to build a near-net-shape part. Like other forms of manufacturing, SFF utilizes heat sources typically used in material joining processes such as gas tungsten arc or electron beam. Most metallic forms of SFF use layer-additive methods for deposition. The process typically uses a computer aided design of two-dimensional slices of a three dimensional part to describe the layer-by-layer deposition of material. Feedstock material can consist of powder, sheet or wire that is melted and fused to the previously deposited layer. There are many forms of this type of manufacturing, including Electron Beam Freeform Fabrication (EBF^3), Laser Engineered Net Shaping (LENS™), Direct Metal Deposition (DMD), and Laser Additive Manufacturing (LAM). These processes are not only used for fabrication of individual components but for repair and salvaging of other parts, or addition of structural details onto simple castings and forgings. Several industries, such as medical and aerospace, benefit from the energy and cost savings afforded by additive manufacturing, primarily due to the use of costly alloys in these fields.

SFF has many advantages over traditional methods of manufacturing, such as energy savings, decreased material waste, shorter design-to-final fabrication time, and increased material properties. Traditional machining and manufacturing methods require certain tolerances and geometries that must be incorporated into the design of the part. These processes can also require expensive consumables for removing material. SFF requires access to only the last

surface layer giving the method a large advantage for tight areas or hollow parts. Casting requires molds, dies and equipment for manufacturing, while SFF requires only a substrate to build upon, decreasing time and cost. The buy-to-fly ratio (ratio of purchased raw material to material used) can be as low as 2:1, where half of the material is used for the final part. Traditional manufacturing methods often result in 14:1 – 20:1 buy-to-fly ratio [1]. Lastly, the deposited microstructure of SFF offers significantly improved mechanical properties, particularly in comparison with cast parts. The localized heating and cooling also restricts chemical segregation, which is frequently observed in thick parts produced in conventional casting.

Many researchers have characterized the microstructure of Ti-6Al-4V material deposited by traditional freeform fabrication methods [2-8]. The typical microstructure consists of the two phases common in Ti-6Al-4V, body centered cubic (BCC) β phase and hexagonal closed packed (HCP) α phase. Using most types of power sources and deposition strategies, large epitaxial β grains are grown in the direction of heat flow during additive manufacturing of Ti-6Al-4V components [2, 8-13]. These large columnar grains grow from the substrate and often result in anisotropic properties [8, 14-16]. Deposition parameters, power source type, consumable attributes and build dimensions can all have an effect on the final microstructure. Beam and arc modulation are common methods of microstructural refinement in traditional fusion welding of Ti-6Al-4V for many reasons, including decreased hot cracking and increased fracture toughness [17-20].

By means of grain refining techniques like beam or arc modulation, mechanical properties may also be dramatically improved. Very limited research has been done on the potential advantages of modulation to SFF [21]. Multiple mechanisms have been proposed regarding the grain refinement of metals during modulated welding. Dendritic fragmentation is the commonly attributed mechanism for grain refinement in modulated weld fusion zones [20, 22]. As the arc current decreases, the weld pool shrinks and the solidification front progresses towards the center of the weld pool at a temporarily increased rate. The solidification front is sensitive to disruptions while advancing towards the center. As the current of the arc then begins to increase, the growing dendrites or entire grains may break from the solidification front and remain solid in the weld pool acting as heterogeneous nucleation sites [23, 24]. However, dendritic fragmentation has been eliminated from the possible mechanisms in Ti-6Al-4V alloy due to the cellular and planar nature of the solidification front, rather than the dendritic solidification commonly observed in aluminum and steel alloys [22]. Increased fluid flow is another mechanism suggested to account for grain refinement due to pulsation from the repeated disruption of arc force. The varied arc forces cause vibrations in the weld pool, constantly adjusting weld pool size [20]. A result from increasing fluid flow and pool agitation is the lowered thermal gradient of the solidification front due to increased mixing [25]. Therefore, the peak thermal gradient of the solidification front is constantly varying, causing a more competitive growth environment and resulting in a relatively large amount of grains growing in small increments. In comparison, only selected grains with preferred orientations grow to a larger extent in conventional welding processes [20, 25, 26].

In this study, the potential of beam and arc modulation are explored to refine the grain size in Ti-6Al-4V deposits fabricated by Electron Beam Freeform Fabrication (EBF^3) and Gas

Tungsten Arc (GTA) deposition, respectively. For each process, a range of process parameters is examined and grain refinement evaluated through quantitative metallographic techniques.

Experimental Procedure

The NASA LaRC EBF^3 machine consists of a 42 kW electron beam welder with a six-axis motion control system and dual wire feeders for wire deposition. The entire 72 in x 24 in x 24 in build volume is contained in a high vacuum environment during deposition. The experimental matrix used to evaluate the effects of beam modulation is shown in Table 1. Powder core tubular wire (PCTW) manufactured at the Colorado School of Mines was used in the EBF^3 system to mitigate vacuum-induced aluminum loss previously observed in the EBF^3 process and correct the net chemical composition of the deposit [1]. The height of deposit, length of deposit, wire feed rate, traverse speed, and accelerating voltage were held constant while beam current, frequency of modulation, and background current were varied to identify the most effective modulation waveform condition and frequency for maximum microstructural refinement. Specific values for the deposition parameters are proprietary, consequently these parameters are shown in a normalized fashion in order to convey the range explored. Two waveform conditions were explored, as shown in Figure 1, each at two modulation frequencies along with a non-modulated baseline. The total heat input was equivalent for both modulation conditions, but slightly lower than the non-modulated build. Both waveform conditions utilize peak current for 50% of the time and utilize background current for the other 50% of the time.

Table 1 Normalized deposition parameters for modulation experiments on EBF^3.

Deposition	Height (in)	Length (in)	Beam Current (Normalized) High	Modulation Freq. (Normalized)	Background Current (%)	Beam Current (Normalized) Low	Fraction of Time at Peak Current (%)	Heat Input (Normalized)
1	0.5	5.0	0.69	0	N/A	N/A	N/A	1
2	0.5	5.0	0.85	0.5f	50	0.43	50	0.90
3	0.5	5.0	1.00	0.5f	25	0..25	50	0.90
4	0.5	5.0	0.85	1.0f	50	0.43	50	0.90
5	0.5	5.0	1.00	1.0f	25	0.25	50	0.90

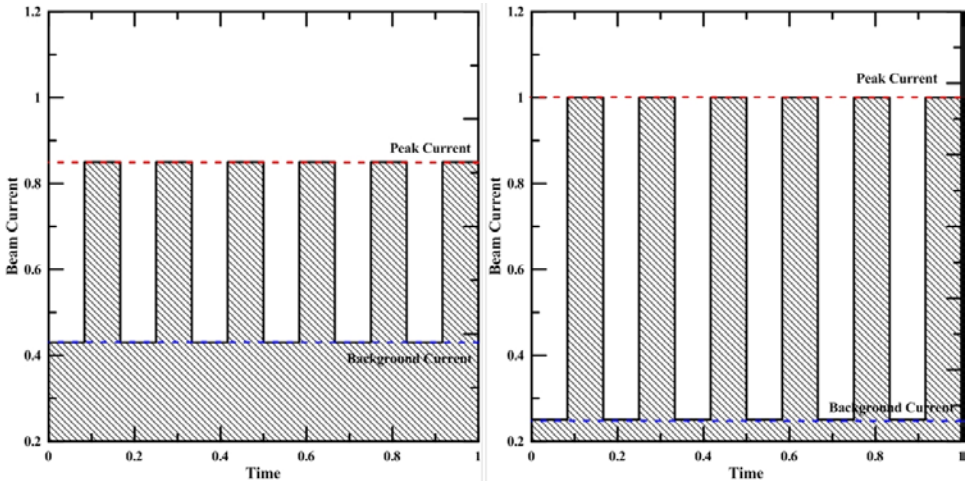

Figure 1 Modulation waveform schematics for use with EBF^3: (a) 50% normalized background current; (b) 25% normalized background current.

Table 2 Deposition parameters for CSM GTA experiments.

Deposition	Height (in)	Length (in)	Arc Current (Normalized) High	Modulation Freq. (Normalized)	Background Current (%)	Arc Current (Normalized) Low	Fraction of Time at Peak Current (%)	Heat Input (Normalized)
1	0.5	5.0	0.82	N/A	N/A	N/A	N/A	0.85
2	0.5	5.0	1.00	N/A	N/A	N/A	N/A	1.00
3	0.5	5.0	0.82	0.12f	40	0.33	1.00	0.85
4	0.5	5.0	0.82	0.24f	40	0.33	1.00	0.85
5	0.5	5.0	0.82	0.48f	40	0.33	1.00	0.85
6	0.5	5.0	0.82	1.00f	40	0.33	1.00	0.85
7	0.5	5.0	1.00	0.12f	40	0.4	0.30	1.00
8	0.5	5.0	1.00	0.24f	40	0.4	0.30	1.00
9	0.5	5.0	1.00	0.48f	40	0.4	0.30	1.00
10	0.5	5.0	1.00	1.00f	40	0.4	0.30	1.00

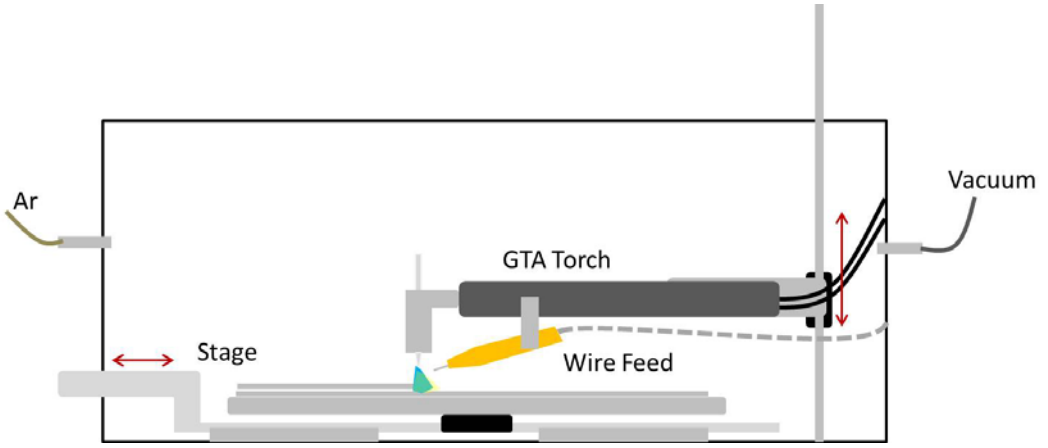

Figure 2Colorado School of Mines GTA freeform fabrication machine schematic.

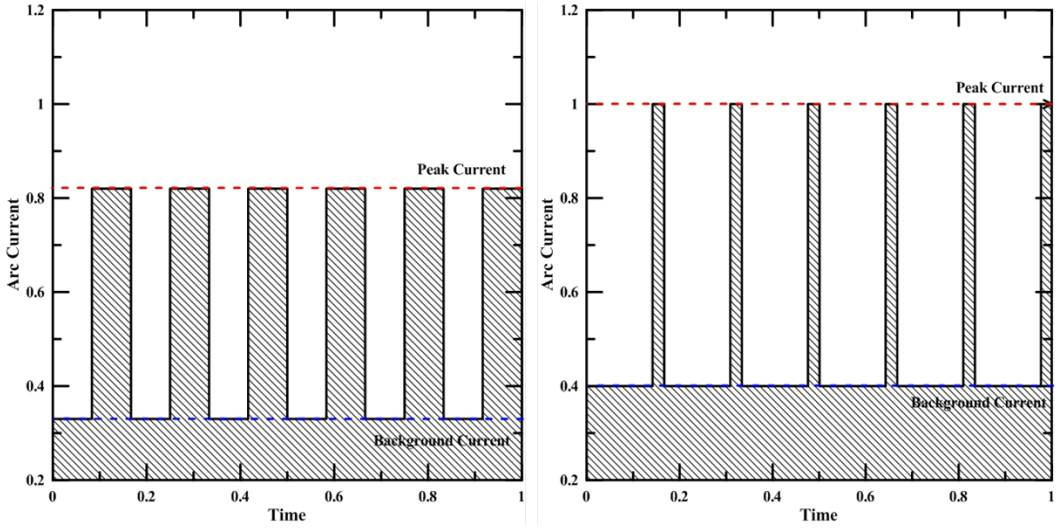

Figure 3 Modulation waveform schematic for CSM GTA machine. (a) 50% background current time (b) 15% background current time.

Upon completion of the wall builds, specimens were cross-sectioned along the Y-Z plane according to the coordinate system illustrated in Figure 4. The cross-sections were mounted in Bakelite and ground through 1200 grit SiC paper. The samples were then polished with 6 μm and 1 μm diamond solutions on green felt and nylon polishing pads, respectively. The samples were then placed on a vibratory polisher with 0.05 μm colloidal silica on a Lecloth pad for the final polish. For the macrographs only, the samples were etched with Kroll's reagent to develop the microstructure for observation using an Olympus PMG3 microscope. Manual and semi-automated metallographic analysis methods were used to characterize four microstructural features identified in literature as having the largest effects on mechanical properties in Ti-6Al-4V alloy [27, 28]. Ti-6Al-4V weld microstructures generally contain two phases, α and β, in a variety of morphologies including globular, basketweave and colony.

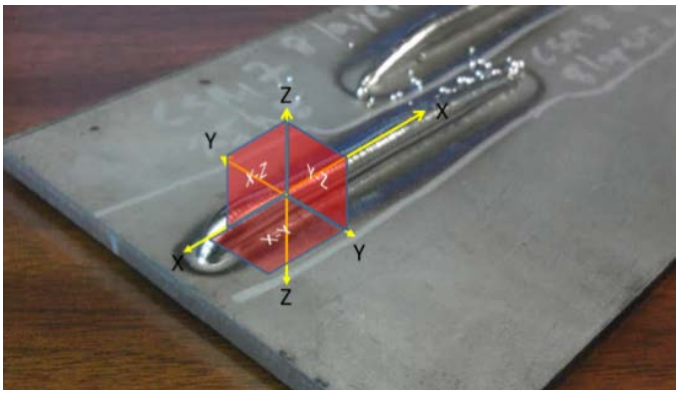

Figure 4 Coordinate system utilized in all experiments.

Two β phase features, grain size and volume fraction were analyzed in the steady-state region of each build. The steady –state region was defined as that portion of the build beginning several layers above the baseplate, where grain morphology should not be affected by the grain structure in the baseplate. The β grain size was characterized using optical macrographs that included a number of grains for suitable statistics. The ImageJ software was used for the analysis using the "Circles" subroutine, which placed circles on the macrographs. A total of 318 circles, placed over the image in a random grid as shown in Figure 5, were used to analyze two macrographs. The intersection of the circle line and the β grain boundaries were then manually counted and an average intercept length calculated as the β grain size using Equation 1.

Equation 1 Calculation of β grain size:

$$\frac{\#\ of\ Intersections}{Total\ Circle\ Line\ Length} = \beta\ Grain\ Size$$

The β phase volume fraction was determined using scanning electron microscope (SEM) back scatter imaging with a JEOL 7000F SEM and the ImageJ software. Five regions were analyzed as follows and as illustrated in Figure 6. The "Find Edges" subroutine was used to identify the regions of β phase, then the image was converted to binary contrast, and the volume fraction of β phase was determined using a macro program.

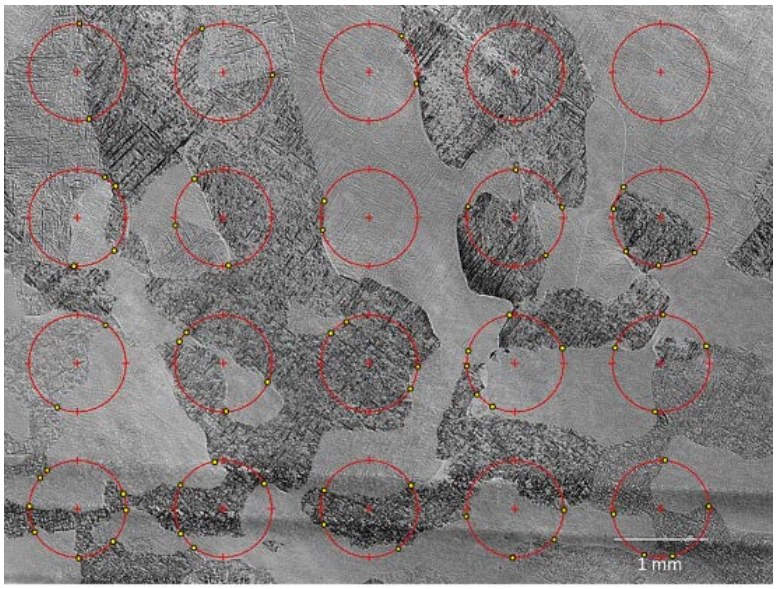

Figure 5 Circular intercept method used for β grain size quantification. Yellow dots represent intersections with β grain boundaries.

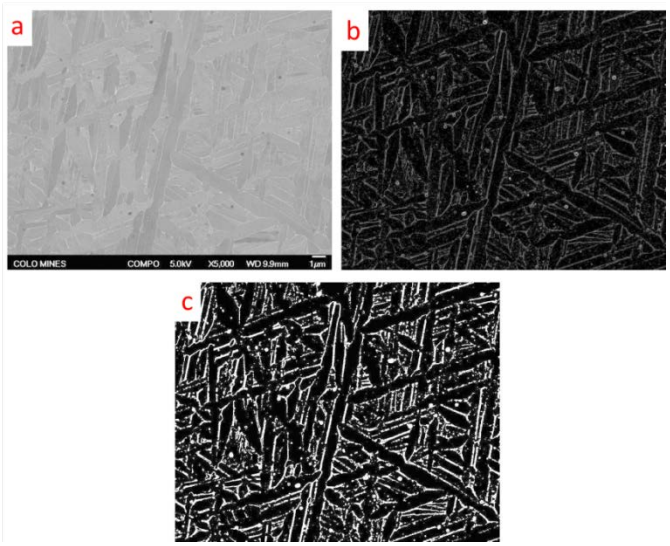

Figure 6 Procedure of β phase fraction analysis: a) Initial backscatter image of an unetched sample showing the chemistry difference of the two phases; b) "Find Edges" command in ImageJ finds the β phase edges in the microstructure; c) Conversion to binary for calculation of β phase fraction.

The α phase colony intercept length and lath width were also characterized in the steady-state region of each build. Figure 7 illustrates the methodology for calculating the average colony intercept length. One hundred random line segments of known length were placed on ten randomly chosen back scatter SEM images and each colony intercept was counted. Using the total number of counts and total line length, an average colony intercept length was found using Equation 2.

Equation 2 Calculation of α colony intercept length:

$$\frac{\#\ of\ Colony\ Intersections}{Total\ Line\ Length} = \alpha\ Colony\ Intercept\ Length$$

The α phase lath width was measured manually using a line segment of known length placed perpendicular to the α phase colony direction, shown in Figure 8. Over 10 random micrographs, 300 laths were measured to find the average lath width for each build. Error analysis was performed according to ASTM E112 standard and the calculated relative accuracy is shown in Table 3. Values less than 10% indicate that these results are accurate. Error bars throughout this paper are represented by the calculated 95% confidence index.

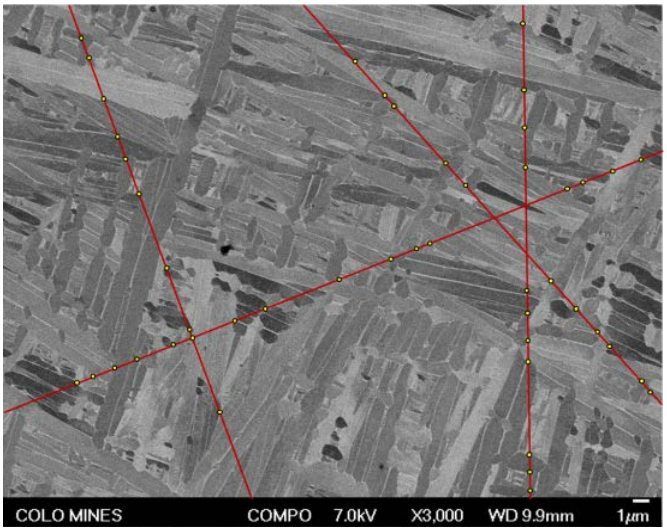

Figure 7 Colony intercept length is determined by the placement of random line segments of known length. At the intersection of two colonies, notice the placement of a yellow dot. The number of the intercepts, yellow dots, per unit line length can be used to find average colony intercept length.

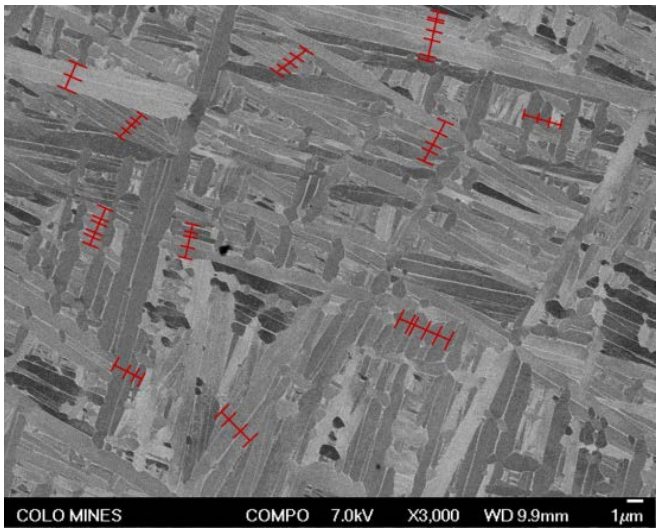

Figure 8 The method of calculating α lath width with perpendicular lines measuring width at the widest point of the lath.

Initial mechanical property evaluation involved microhardness testing of the steady-state region of each build in all three planes: X-Z, Y-Z, and X-Y. Cross-sections were made through each section and prepared in the same manner as described earlier for microstructural characterization, through 0.05 μm colloidal silica, but these samples were not etched. Fifteen random Vickers hardness indentions in the steady-state region were completed with a Leco MHT Series 200 microhardness machine on each of the three planes for each build. Indentions were performed with a 10 second dwell time and a 500 gram load.

Table 3 Average relative accuracy of the quantification of microstructural features. Readings with 10% or less are considered accurate [29].

Characterized Feature	Average Relative Accuracy (%)
β Phase Volume Fraction	8.8
α Phase Colony Intercept Length	9.0
α Phase Lath Width	10.1
β Phase Grain Size	6.8

Results and Discussion

Beam modulation during Electron Beam Freeform Fabrication:

Electron beam modulation was implemented with a consistent 50% background time waveform condition; however, the background current was varied at 50% and 25% of the peak current to investigate the effect of modulation condition. It should be noted that the traditional, non-modulated builds had a slightly higher heat input than the beam modulated builds. All plots refer to the traditional non-modulated builds as a normalized frequency of modulation of 0.

β Phase Refinement:

With modulation, the traditional long columnar grains typical of electron beam freeform fabrication (EBF^3) were modified to a much more equiaxed structure. Fresh grains were found to nucleate in the steady-state region of the build, where epitaxial growth normally predominates, as seen in Figure 9. The β grain size was drastically reduced for both modulation waveform conditions, for example, from 1164 μm to 734 μm with the 25% background current, as shown in Figure 10. Accordingly, volume fraction of β phase increased with modulation, from 22.7% to 35.0%, with the peak increase of β phase seen at the highest modulation frequency. Utilizing backscatter micrographs shown in Figure 11, the variance of phase types can be observed.

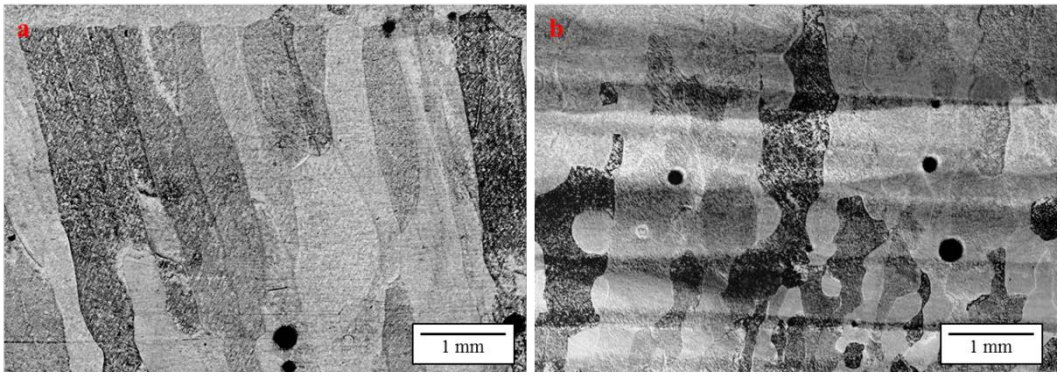

Figure 9 β grain size refinement (a) Non-modulated (b) Modulation per deposition conditions for deposit 5 in Table 1.

α Phase Refinement:

The refinement of α phase was observed for both frequencies, with the most refinement at the highest modulation frequency. Figure 12 shows representative micrographs for non-modulated and modulated builds. The microstructure for both the non-modulated and the modulated builds is primarily composed of fine colony α phase morphology with small areas of basketweave morphology. Figure 13 shows the refinement of the α phase due to modulation, as indicated by the reduction in α colony intercept length from 3.2 μm to 2.2 μm. The α lath width has also been refined by half, from 1.0 μm to 0.5 μm, also shown in Figure 13.

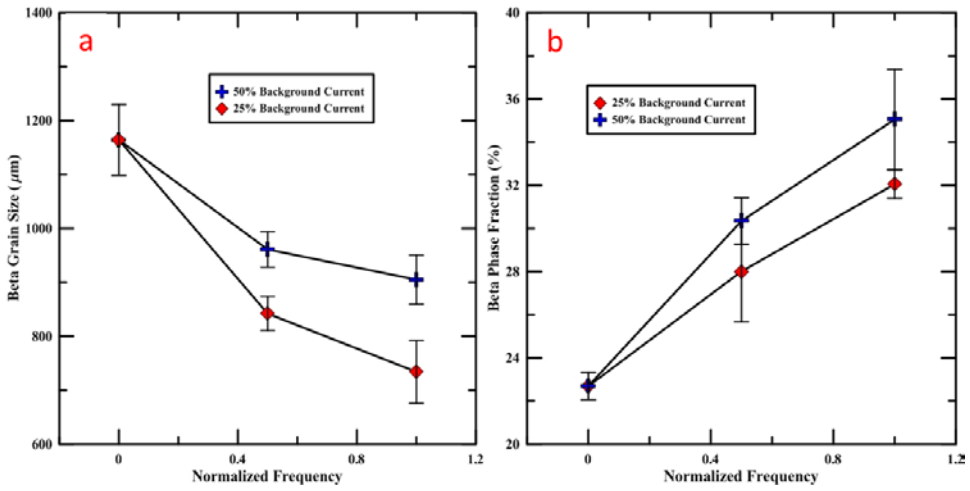

Figure 10 β grain size, (a), refinement using modulation for each waveform condition. Peak grain size refinement was observed at maximum modulation frequency. β phase volume fraction (b) was increased from 22.7% to 35.0%.

Microhardness of modulated EBF^3 Builds:

The mechanical response to the refinement in microstructure was measured with Vickers microhardness. Each plane, X-Z, Y-Z, and X-Y was analyzed to estimate mechanical properties in each direction. Figure 14 shows that hardness in all planes increased due to microstructure refinement, with the Y-Z plane showing an increase from 325 VHN to 356 VHN. Figure 14 also shows an increase in hardness for the X-Z and X-Y planes from 338 VHN to 353 VHN and 343

VHN to 356 VHN, respectively. The peak microstructural refinement occurred in the 25% background current waveform condition and peak hardness was consistent between the two modulation conditions. Consistent with the changes in α and β phases with frequency, hardness continued to increase over the range of frequencies examined. Figure 15 illustrates the improved material isotropy. The non-modulated builds, highlighted in the red boxes, yielded mixed hardness values for the three planes, while the moderate frequency for both modulation conditions yielded consistent increases in hardness over all planes. Frequency seems to have the largest effect on hardness, as the observed hardness variation between the two waveform conditions was small.

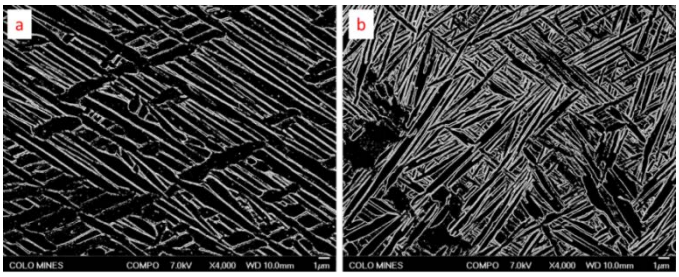

Figure 11 β phase fraction (a) Non-modulated (b) Modulation per deposition conditions for deposit 5 in Table 1.

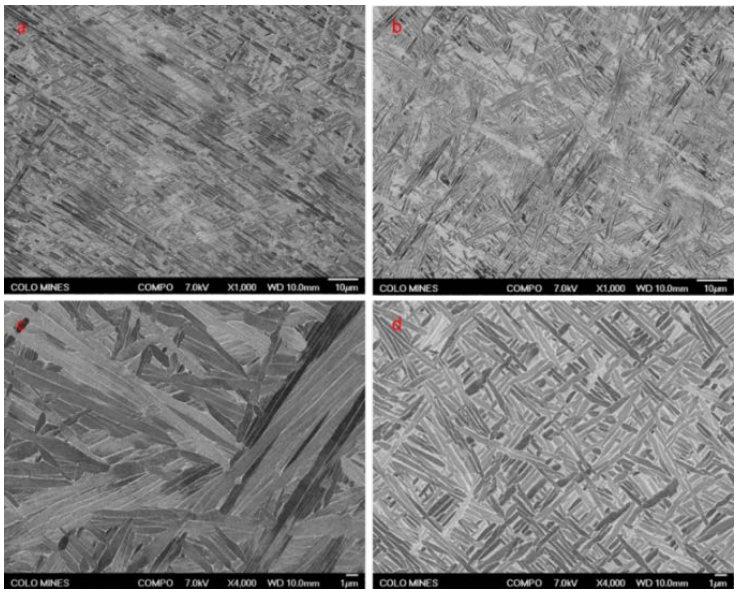

Figure 12 Refinement achieved through modulation per deposition conditions for deposit 5 in Table 1: (a) baseline build with no modulation at lower magnification; (b) modulated build at lower magnification; (c) baseline build with no modulation at high magnification; (d) modulated build at high magnification.

The Hall-Petch relationship is a method for determining how microstructure and mechanical properties impact each other using the relationship in Equation 3 [30]. Utilizing α lath width in the Y-Z plane as the characteristic distance, d, Figure 16 shows the good correlation between this relationship and the data. The regression coefficient R is 0.963 indicating the measured α width is a just assumption of the microstructural-microhardness relationship.

Equation 3 **Hall-Petch relationship, where VHN is the hardness number and d is the characteristic distance (usually grain size):**

$$VHN \propto \frac{1}{\sqrt{d}}$$

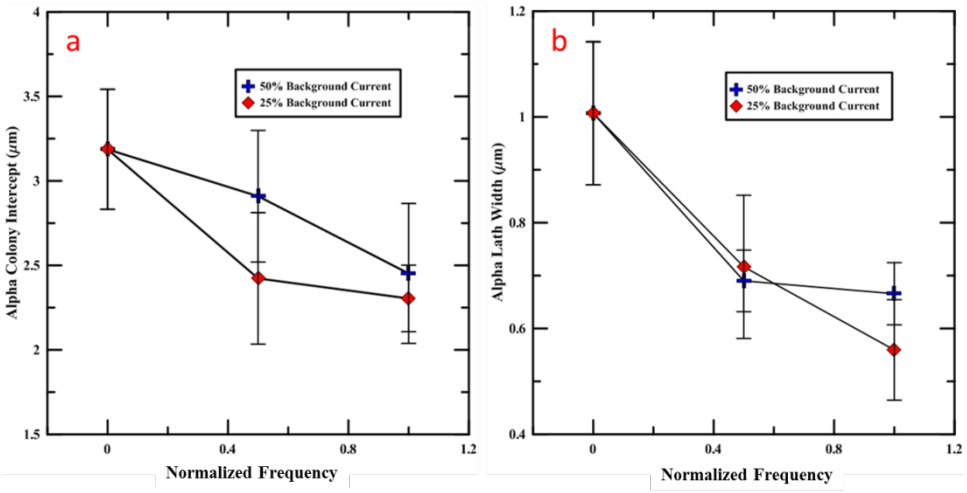

Figure 13 **α colony intercept lengths (a) and α lath width (b) for both modulated conditions. Peak refinement and smallest lath spacing occurs for the deposition conditions for deposit 5 in Table 1.**

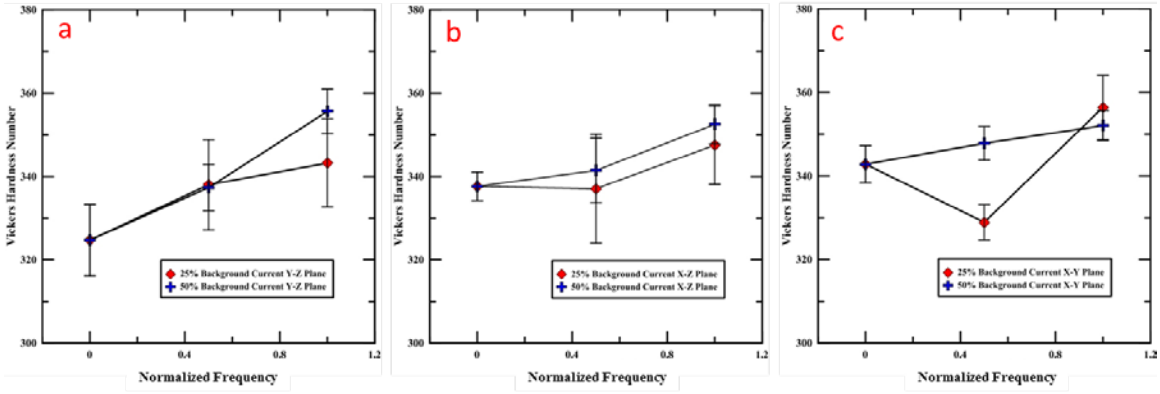

Figure 14 **Variation in microhardness with frequency measure in (a) Y-Z plane, (b) X-Z plane, and (c) X-Y plane.**

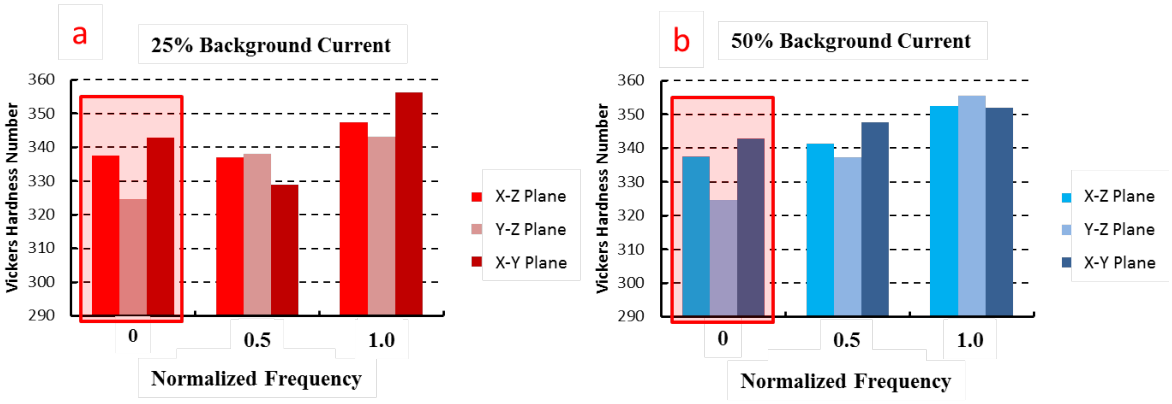

Figure 15 **Bar plot showing the hardness in each direction with non-modulated builds highlighted by the red boxes. Hardness has been increased for all directions, resulting in more isotropic values. (a) Shows the 25% background current waveform condition (b) Shows the 50% background current waveform condition.**

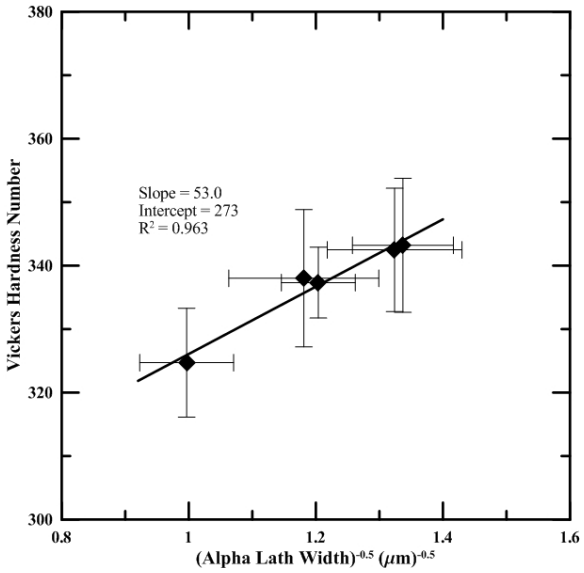

Figure 16 **Hall-Petch relationship utilizing α width. The regression coefficient of 0.96 indicates a strong linearity of the data.**

Arc modulation during Gas-Tungsten Arc freeform fabrication:

Two modulation waveform conditions were utilized for the GTA deposits. In contrast to the EBF[3] builds, which varied the background current while keeping the time at a constant 50% peak current time and 50% background current time, the GTA builds kept the background current constant at 40% of the peak current while varying the time at peak current. The two peak current times used were 50% peak current time and 15% peak current time to magnify the possible effects from modulation. Baseline builds were made with traditional non-modulated parameters. For all builds, parameters were varied in order to keep the total heat input constant to eliminate any possible effects from a change in heat input. All plots refer to the traditional non-modulated builds as a normalized frequency of modulation of 0.

β Phase Refinement:

Refinement of the large β grains found in non-modulated builds was successfully accomplished with both modulated waveform conditions. Figure 17 shows the morphology change due to the modulated arc. Similar to the EBF^3 builds, epitaxial grain growth was still evident in the modulated builds; however new grains with much more equiaxed shape were found in the steady-state region. Figure 18 shows the change in β grain size as a function of frequency for both modulation conditions. In contrast to the EBF^3 builds, the greatest degree of refinement occurred at an intermediate frequency of modulation. During the higher frequency builds the weld pool did not have sufficient time to change shape, likely due to the weakening effect of weld pool agitation, therefore the mechanism of grain refinement was inhibited. At peak refinement the β grain size decreased from 1450 μm to 980 μm, which is consistent with literature data [20]. A representative micrograph of the increase in β phase volume fraction is shown in Figure 19. The peak in β phase volume fraction, as shown in Figure 18, occurred at the same modulation waveform condition as the minimum in β grain size. The fraction of β phase increased from 14.7% to 24.6%. A decrease in β phase volume fraction was observed at the high frequencies, which is consistent with the evidence of loss of the grain refining mechanism observed for the β grain size measurements.

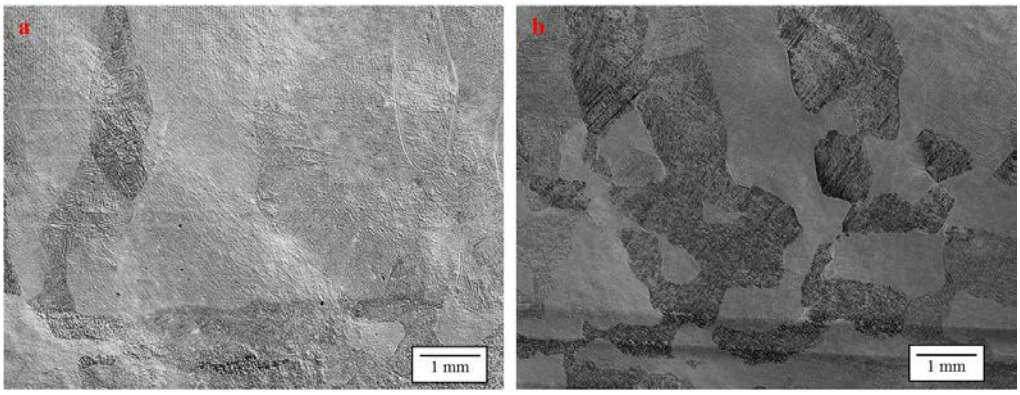

Figure 17 **β grain refinement due to arc modulation (a) Non-modulated build (b) Modulated arc as described for deposition 8 in Table 2.**

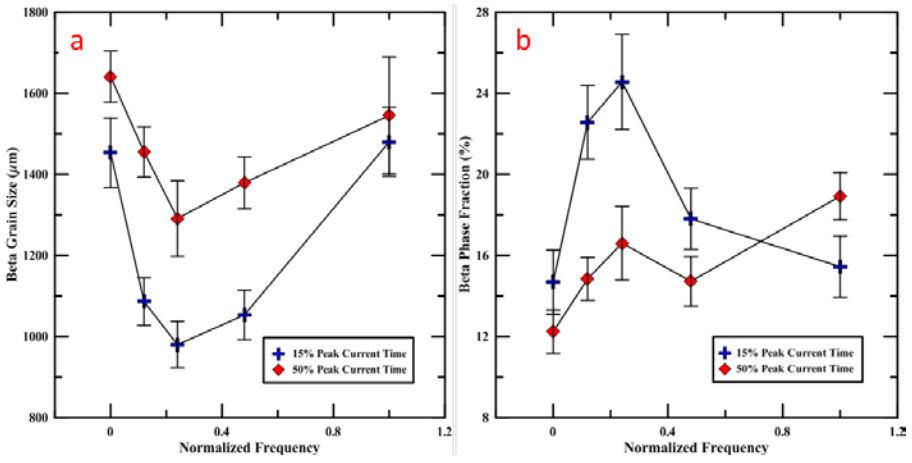

Figure 18 **β phase refinement due to arc pulsation (a) β grain size for both modulation conditions. (b) β phase volume fraction increase for both waveform conditions.**

α Phase Refinement:

The effect of modulation on α phase morphology was characterized by α colony intercept length and α lath width. Representative backscatter electron micrographs are shown in Figure 20. Similar to the β phase refinement, a similar trend of peak refinement at an intermediate frequency followed by coarsening at higher frequencies was observed for α colony intercept length, as shown in Figure 20. The peak refinement occurred at the same conditions as for β phase refinement, with α colony intercept length reduced from 2.9 μm to 2.2 μm as compared with the non-modulated build. Figure 21 also shows that α lath width decreased with increasing frequency for both of the modulated conditions; however the behavior of α lath width did not show the microstructural coarsening in higher frequencies shown in the previous quantified features. Due to the theoretical maximum colony intercept length having dependence on β grain size, it is not surprising that the trend of colony refinement is similar to the β grain size trend. The α lath trend is unique, however, as it showed a constant refinement over all frequencies of modulation.

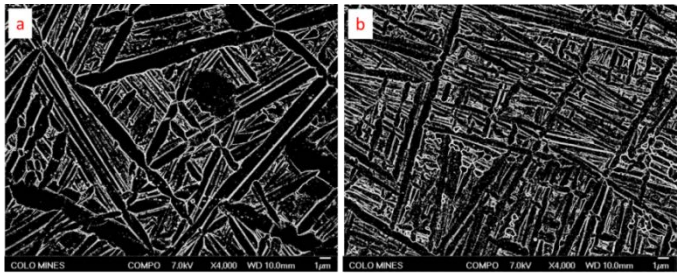

Figure 19 **Representative change in β phase fraction with arc modulation. (a) Non-modulated builds parameters (b) Arc modulation as described for deposit 8 in Table 2.**

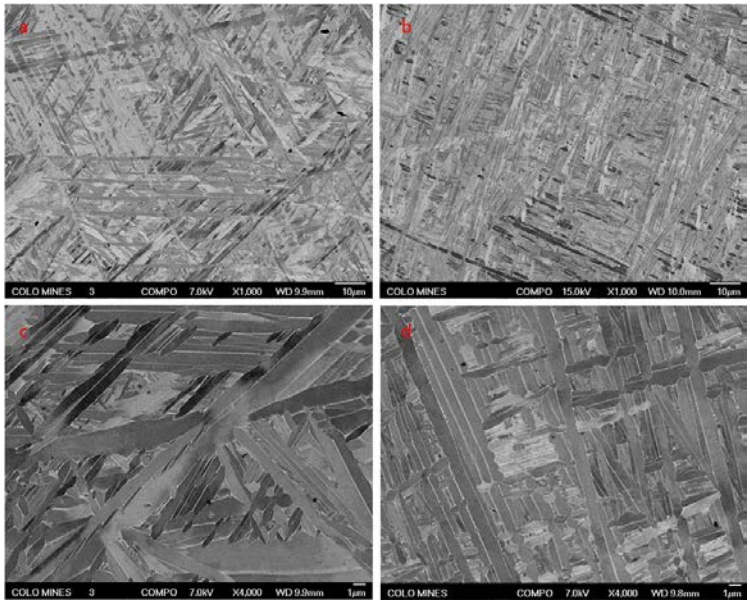

Figure 20 **Refinement of α phase due to arc modulation. (a) Baseline build with no modulation at low magnification (b) Modulated build at low magnification (c) Baseline build with no modulation at high magnification (d) Modulated build at high magnification.**

Microhardness of modulated GTA freeform fabrication builds:

Microhardness was used to determine the effect of arc modulation and resulting grain refinement on material properties. Hardness on each of the planes, Y-Z, X-Z, and X-Y was measured as an indication of changes in strength and to examine anisotropy within the builds. The trend in hardness was similar for all planes and for both waveform conditions, as shown in Figure 22. All the arc-modulated builds displayed beneficial increases in hardness as compared with the baseline, non-modulated build. The trend in microhardness was similar to that observed for α lath width, characterized by a rapid change with arc modulation at the lowest frequency followed by a plateau in values for subsequent increase in frequency. The degree of anisotropy for each waveform condition is shown in Figure 23. A high degree of anisotropy is evident in the builds made with traditional non-modulated parameters, highlighted in red boxes in Figure 23. Arc modulation resulted in increased hardness for nearly all planes, and significantly reduced anisotropy. Hall-Petch analysis was conducted for α lath width and microhardness for the Y-Z plane, and the results are plotted in Figure 24. The plot shows a good agreement between microhardness and α lath width, with a linear regression coefficient R^2 of 0.90.

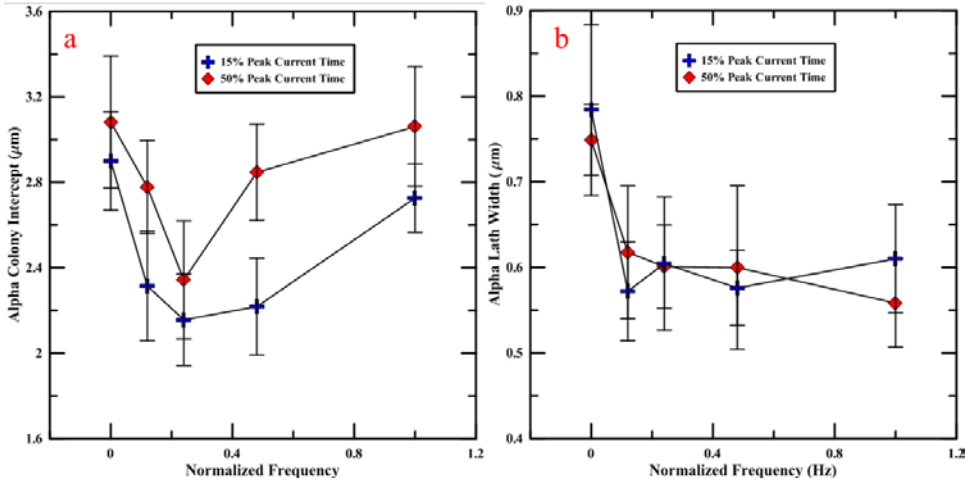

Figure 21 **Trend in α phase refinement with frequency. (a) α colony intercept lengths for both modulated conditions. (b) α lath width for both modulation conditions.**

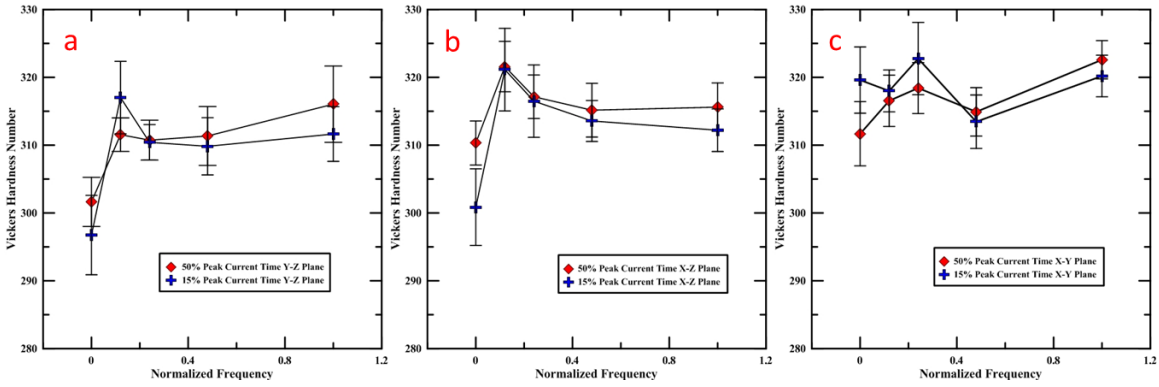

Figure 22 **Variation in microhardness with frequency measure in (a) Y-Z plane, (b) X-Z plane, and (c) X-Y plane.**

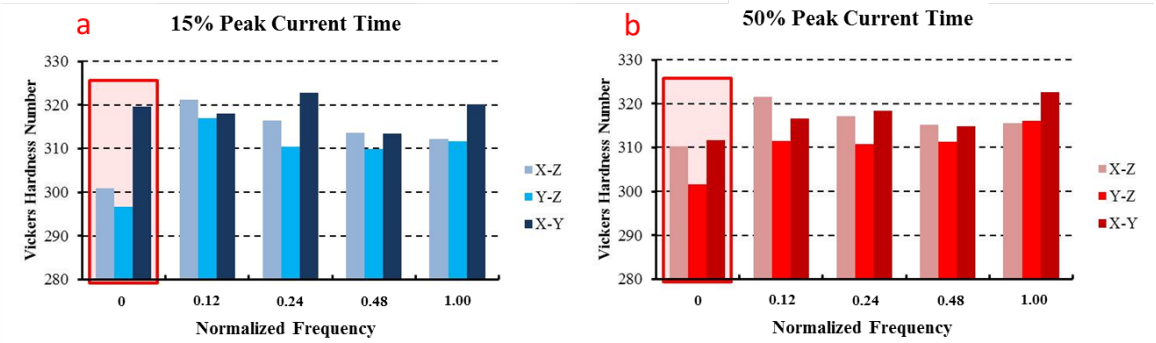

Figure 23 **Bar plot showing the hardness in each direction with non-modulated builds highlighted by the red boxes. Hardness was increased by arc modulation in all directions, resulting in a more isotropic specimen. (a) 15% peak current time waveform condition, (b) 50% peak current time waveform condition.**

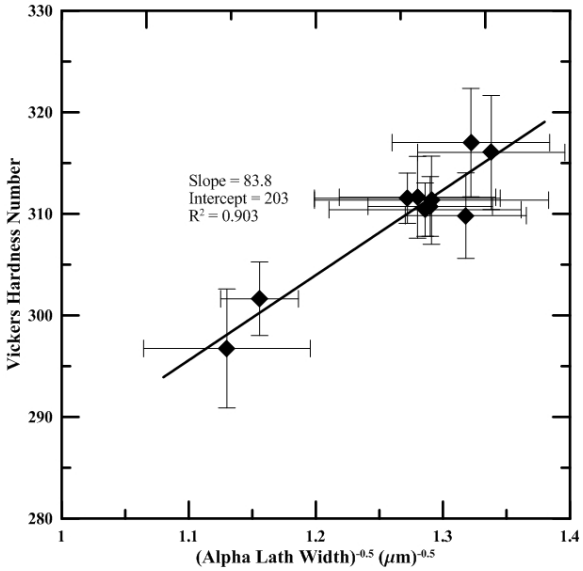

Figure 24 **Hall-Petch relationship of α lath width to VHN. The linear regression coefficient of 0.90 indicates a good linear relationship.**

Conclusions

Microstructural refinement and improved mechanical isotropy in Ti-6Al-4V alloy builds was successfully demonstrated with changes to deposition parameters for both the EBF^3 system at NASA LaRC and the GTA freeform fabrication machine at the Colorado School of Mines. The main conclusions drawn from this work are the following:

1. Deposition using the EBF^3 system showed a trend of continuously increasing grain refinement with beam modulation frequency, with peak refinement at the maximum frequency examined. β grain size decreased from 1160 μm to 730 μm and β phase volume fraction increased from 22.7% to 35.0%. The α phase colony intercept length and α lath width were also refined from 3.2 μm to 2.2 μm and from 1.0 μm to 0.5 μm, respectively.
2. Deposition using the GTA freeform fabrication system resulted in maximum grain refinement at an intermediate modulation frequency, with coarsening at higher

frequencies. β grain size decreased from 1450 μm to 980 μm and β phase volume fraction increased from 14.7% to 24.6%. The α phase colony intercept length and α lath width was also refined from 2.9 μm to 2.2 μm and from 0.8 μm to 0.6 μm, respectively.

3. Both modulated energy sources resulted in higher hardness values for Ti-6Al-4V alloy builds, with hardness increasing overall from 325 VHN to 356 VHN using modulation in the EBF^3 machine and from 300 VHN to 321 VHN using modulation in the GTA machine. The changes in hardness also resulted in enhanced isotropy in the builds, an indication of improved uniformity in mechanical properties within the builds. A strong correlation was observed between hardness and α lath width using the Hall-Petch relationship.
4. Dissimilarities between the two processes may be related to the differences in the power sources and wire consumables. The electron beam deposition method in the EBF^3 system uses a rastering, high-density heat source and since the process occurs in high vacuum, requires the use of custom alloyed PCTWs for accurate deposition chemical composition. The CSM GTA system uses a traditional, relatively low-density GTA torch as the heat source and used conventional solid-core wire with unmodified chemistry.. These variances may explain the different grain refinement-frequency trends and Hall-Petch parameters.

Acknowledgements

The authors acknowledge the support of the Advanced Materials and Processing Branch at NASA Langley Research Center and the use of the EBF^3 system. One of the authors (S.M.) would also like to acknowledge the assistance of graduate students of the Colorado School of Mines Center for Welding, Joining and Coating Research Group.

References

[1] C. Hillier, "Powder-Cored Tubular Wire Development for Electron Beam Freeform Fabrication," Department of Metallurgical and Materials Engineering, Colorado School of Mines, Golden, 2010.

[2] B. Baufeld, O. V. d. Biest, and R. Gault, "Additive manufacturing of Ti-6Al-4V components by shaped metal deposition: Microstructure and mechanical properties," *Materials & Design,* vol. 31, pp. S106-S111, 2010.

[3] E. Brandl, V. Michailov, B. Viehweger, and C. Leyens, "Deposition of Ti–6Al–4V using laser and wire, part I: Microstructural properties of single beads," *Surface and Coatings Technology,* vol. 206, pp. 1120-1129, 2011.

[4] L. E. Murr, S. A. Quinones, S. M. Gaytan, M. I. Lopez, A. Rodela, E. Y. Martinez*, et al.*, "Microstructure and mechanical behavior of Ti-6Al-4V produced by rapid-layer manufacturing, for biomedical applications," *Journal of the Mechanical Behavior of Biomedical Materials,* vol. 2, pp. 20-32, 2009.

[5] F. Wang, J. Mei, and X. Wu, "Microstructure study of direct laser fabricated Ti alloys using powder and wire," *Applied Surface Science,* vol. 253, pp. 1424-1430, 2006.

[6] E. Brandl, A. Schoberth, and C. Leyens, "Morphology, microstructure, and hardness of titanium (Ti-6Al-4V) blocks deposited by wire-feed additive layer manufacturing (ALM)," *Materials Science and Engineering: A,* vol. 532, pp. 295-307, 2012.

[7] J. Alcisto, A. Enriquez, H. Garcia, S. Hinkson, T. Steelman, E. Silverman*, et al.*, "Tensile Properties and Microstructures of Laser-Formed Ti-6Al-4V," *Journal of Materials Engineering and Performance,* vol. 20, pp. 203-212, 2011.

[8] B. Baufeld, E. Brandl, and O. van der Biest, "Wire based additive layer manufacturing: Comparison of microstructure and mechanical properties of Ti-6Al-4V components fabricated by laser-beam deposition and shaped metal deposition," *Journal of Materials Processing Technology,* vol. 211, pp. 1146-1158, 2011.

[9] T. Hua, C. Jing, Z. Fengying, L. Xin, and H. Weidong, "Microstructure and Mechanical Properties of Laser Solid Formed Ti-6Al-4V from Blended Elemental Powders," *Rare Metal Materials and Engineering,* vol. 38, pp. 574-578, 2009.

[10] S. M. Kelly and S. L. Kampe, "Microstructural Evolution in Laser-Deposited Multilayer Ti-6Al-4V Builds: Part I. Microstructural Characterization," *Metallurgical and Materials Transactions A,* vol. 35A, pp. 1861-1867, 2004.

[11] S. Bontha, N. W. Klingbeil, P. A. Kobryn, and H. L. Fraser, "Effects of process variables and size-scale on solidification microstructure in beam-based fabrication of bulky 3D structures," *Materials Science and Engineering: A,* vol. 513-514, pp. 311-318, 2009.

[12] S. Semiatin, P. Kobryn, E. Roush, D. Furrer, T. Howson, R. Boyer*, et al.*, "Plastic flow and microstructure evolution during thermomechanical processing of laser-deposited Ti-6Al-4V preforms," *Metallurgical and Materials Transactions A,* vol. 32, pp. 1801-1811, 2001.

[13] L. Thijs, F. Verhaeghe, T. Craeghs, J. V. Humbeeck, and J.-P. Kruth, "A study of the microstructural evolution during selective laser melting of Ti–6Al–4V," *Acta Materialia,* vol. 58, pp. 3303-3312, 2010.

[14] B. Baufeld, O. V. d. Biest, and R. Gault, "Additive manufacturing of Ti–6Al–4V components by shaped metal deposition: Microstructure and mechanical properties," *Materials & Design,* vol. 31, Supplement 1, pp. S106-S111, 2010.

[15] E. Brandl, B. Baufeld, C. Leyens, and R. Gault, "Additive manufactured Ti-6Al-4V using welding wire: comparison of laser and arc beam deposition and evaluation with respect to aerospace material specifications," *Physics Procedia,* vol. 5, pp. 595-606, 2010.

[16] P. A. Kobryn and S. L. Semiatin, "Mechanical Properties of Laser-Deposited Ti-6Al-4V," in *SFF Symposium Proceedings*, 2001, pp. 179-186.

[17] S. Kou, "Welding Metallurgy," 2nd ed. New Jersey: John Wiley & Sons Inc, 2003.

[18] M. Balasubramanian, V. Jayabalan, and V. Balasubramanian, "Effect of microstructure on impact toughness of pulsed current GTA welded α–β titanium alloy," *Materials Letters,* vol. 62, pp. 1102-1106, 2008.

[19] M. Balasubramanian, V. Jayabalan, and V. Balasubramanian, "Effect of pulsed gas tungsten arc welding on corrosion behavior of Ti–6Al–4V titanium alloy," *Materials & Design,* vol. 29, pp. 1359-1363, 2008.

[20] S. Sundaresan, G. D. Janaki Ram, and G. Madhusudhan Reddy, "Microstructural refinement of weld fusion zones in [alpha]-[beta] titanium alloys using pulsed current welding," *Materials Science and Engineering: A,* vol. 262, pp. 88-100, 1999.

[21] F. Wang, S. Williams, and M. Rush, "Morphology investigation on direct current pulsed gas tungsten arc welded additive layer manufactured Ti6Al4V alloy," *The International Journal of Advanced Manufacturing Technology,* vol. 57, pp. 597-603, 2011.

[22] D. L. Hallum and W. A. Baeslack III, "Nature of Grain Refinement in Titanium Alloy Welds by Microcooler Inoculation," *Welding Journal,* vol. 9, pp. 326-336, 1990.

[23] S. Kou and Y. Le, "Nucleation Mechanisms and Grain Refining of Weld Metal," *Welding Journal,* vol. 12, pp. 305-313, 1986.
[24] B. Pearce and H. Kerr, "Grain refinement in magnetically stirred GTA welds of aluminum alloys," *Metallurgical and Materials Transactions B,* vol. 12, pp. 479-486, 1981.
[25] G. Reddy, A. Gokhale, and K. Rao, "Weld microstructure refinement in a 1441 grade aluminium-lithium alloy," *Journal of Materials Science,* vol. 32, pp. 4117-4126, 1997.
[26] G. D. Janaki Ram, T. K. Mitra, M. K. Raju, and S. Sundaresan, "Use of inoculants to refine weld solidification structure and improve weldability in type 2090 Al---Li alloy," *Materials Science and Engineering A,* vol. 276, pp. 48-57, 2000.
[27] T. Searles, J. Tiley, A. Tanner, R. Williams, B. Rollins, E. Lee*, et al.*, "Rapid characterization of titanium microstructural features for specific modeling of mechanical properties," *Measurement Science and Technology,* vol. 16, 2004.
[28] J. Tiley, T. Searles, E. Lee, S. Kar, R. Banerjee, J. C. Russ*, et al.*, *Material Science and Engineering A,* vol. 372, 2004.
[29] *ASTM E112-2004, Standard Test Methods for Determining AverageGrain Size* vol. 2008: ASTM.
[30] G. Dieter, *Mechanical Metallurgy*, 3rd ed. U.S.A.: McGraw-Hill, 1986.